Supplement of Atmos. Meas. Tech., 13, 7069–7096, 2020
https://doi.org/10.5194/amt-13-7069-2020-supplement

Atmospheric Measurement Techniques
Open Access
EGU

Supplement of

Emissions relationships in western forest fire plumes – Part 1: Reducing the effect of mixing errors on emission factors

Robert B. Chatfield et al.

Correspondence to: Meinrat O. Andreae (m.andreae@mpic.de) and Robert B. Chatfield (chatfield@alumni.rice.edu)

Note on EnRs and ERs. (Section 1): Most often, ER < EnR, as attack by photooxidants reduces the emitted species, decreasing with the concentration of emitted fire product *j,* Δy_j in the the numerator $\mathrm{EnR}_j = \Delta y_j/\Delta x$. Aerosol properties like scattering coefficient may decrease as particles coagulate, so that the ration of the volume to the scattering-determining cross section decreases. Some EnRs describe species like ozone, not present in flame, or nitric acid and PAN, not present at high levels. A textbook understanding of organic compound oxidation and the literature suggest that formaldehyde experiences thermochemical production in the flame, decay by photochemical processes, processes that overwhelm significant continued production. For use of emission factors in modeling, the circumstances of emission need to be described clearly, and the ER must be a true result of emissions. The conversion of ERs to EFs requires a separate analysis of carbon in the wood biomass, factors like area burned, the wood distribution in the area, its carbon versus water content, etc. (Andreae and Merlet, 2001, Yokelson et al. 2007). This analysis can vary from fire to fire. Such analyses can also determine the N content of the biomass burned, and this is useful in understanding the emission of nitrogen compounds.

Note on CO Fill-in (Section 2): In order to provide a suitably complete dataset for SEAC4RS, we used the can samples to infer likely concentrations at one-minute intervals of key species, i.e., CH_4 for all flights and CO for the first few flights, using available can samples at slightly lower frequency. The **R** package for multiple imputations by chained equations (*mice()*) was employed, using the whole data period, but filling in observations with missing data. (Our assessment of the effect of imputation was informal and is reviewed again below.) It was highly desirable to include the imputed concentrations of methane, since it is commonly measured and appears to be a prominent signal of different types of "fire chemistry", i.e., enhanced emission of reduced species; methanol and acetone are often correlated with CH_4 and give support to this idea.

The use of imputation seemed justified by three observations: (1) Checks made when both LAS and GC data were available suggested agreement. In an early period, missing tunable-laser absorption spectrometry data for both CO and CH_4, some periods did not pass this test and all observations from this period were deleted. (2) The use of regression in both mice() and succeeding emission ratio analyses suggested that when observations were filled in, very little information was added, i.e., if the technique allowed missing observations, the results would be extremely similar. CH_4 was omitted from tracer variables used since its cumulative probability distribution, differing from 8 others, suggested non-burning effects that could not be removed. (3) Comparisons of 10-second and 1-minute averages for the more detailed ARCTAS dataset (not reported here) suggested that the essential variability had been captured by 60-second data. We surmised that 30-second averages might have captured more. We are unsure how averaging affects difference-based methods.

Note on Volumes (Section 3): For example, the sequence of increasingly large boxes in Figure 5 emphasizes that the relative effect of entrained non-fire air is largest near the flames, but the absolute effect of entrained air on the composition of an observed parcel is often largest close to the parcel at its point of sampling. The following section gives a framework illustrating effects of emissions and entrainment on EnRs. The box volumes of parcels at different altitudes are similar to the mole amounts shown; to be consistent with adiabatic rise of parcels, volumes should be about ~11%-14% larger in linear dimension for most plume tops)

Note on Initial Point (Section 4.1): It is natural to ask where this time/molar-expansion integration should start, naming it as $\nu = \nu_1$. A reasonable start location is *when the fire plume parcels begin entraining predominantly environmental air*, not other fresh emissions. The plume that is characterized by this expansion-period analysis is then that mixture over space and time of all detailed variations in emissions before this transition. We remark that emissions from the very hottest flaming combustion in a fire front are likely mixed with neighboring fumes from less vigorous combustion. The hottest regions seem likely never to be directly sampled. Their relevance to all downwind processing and effects is only as part of a mixture. In our dataset, the very hottest burns, MCE > 0.97, were very rarely sampled. We speculate that values of x and y_{CO}, which represent the MCE during true flaming combustion, may typically be confined to a region very close to the fire, which is measurable in the laboratory but rarely in the field.

Note on Varying Entrainment: As a side note, in simple situations (e.g., observations in a plume with same environment but with decreasing dilution, from upwind to downwind), the equation reduces to

$$\left(y_{\alpha j} - y_{\beta j}\right) = a_j \left(x_\alpha - x_\beta\right) \tag{13}$$

for any two observational instances, α and β, in the same plume. These are supposed chosen so that we know that x^E and all the y_j^E remain constant. If there is different dilution in the next stage, say instances β and γ, a similar relation obtains, and the composite retains linearity. Questions regarding constants of integration and original concentrations at *a* can be resolved in the regression procedure, Section 5. More generally we need $\left|x^{E\alpha} - x^{E\beta}\right| \ll \left|x_\alpha - x_\beta\right|$ and $\left|y_j^{E\alpha} - y_j^{E\beta}\right| \ll \left|y_{\alpha j} - y_{\beta j}\right|$. Situations in which the entraining concentrations vary are described later in Figure 6d. All these observations invite a more general theoretical statement, one that is necessarily more complex and is appropriate for later work.

Note on an Early Approximate C_{burn}

After having calculated a normalization as in Equation 21 one can see an approximate description of C_{burn}, and the the ratioing variable can be given the approximate magnitude of C_{burn} and in the same units. We found that the mid-range of values of C_{tot} and ν_i gave the best calibration and used order statistics to define the calibration in terms of ppm. Low values of C_{tot} can be affected by measurement precision, and the highest values suffer from the scattered nature of the statistics of extremes.

$$\nu_i = \underset{j}{\mathrm{mean}}\left(y_{ij}\right) \qquad \left(C_{\mathrm{burn}}^{\mathrm{Approx}}\right) = \underset{j}{\mathrm{mean}}\left(y_{ij}\right) \frac{\left(Q(C_{\mathrm{tot}})_j^{75} - Q(C_{\mathrm{tot}})_j^{25}\right)}{\left(Q(y)_j^{75} - Q(y)_j^{25}\right)}$$

(For our situation, where we expected rather different environmental or background values between ARCTAS and SEAC4RS of both CO_2 and CO based on year and season, we use individual values of the numerator involving C_{tot} for each period.)

Note on Sensitivity to Number of Tracers Used (Section 7)

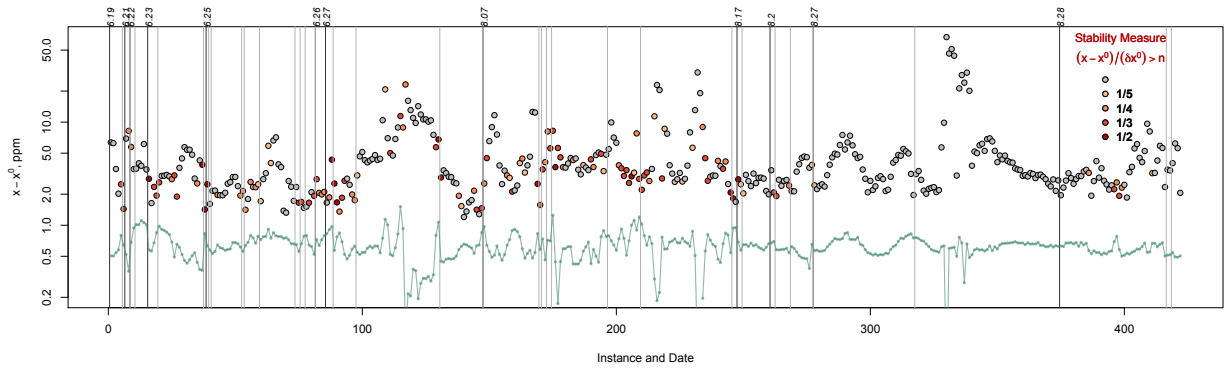

Figure S1: Estimate of variation in C_{burn} if x^0 is estimated by only three tracers (green dots:) and only five tracers (red dots). Green line repeats the pattern of $\widehat{\boldsymbol{x}}_{\boldsymbol{i}}^{\boldsymbol{0}} = C_{\text{bkgd}}$ shown with appropriate scale in Figure 8, for reference.

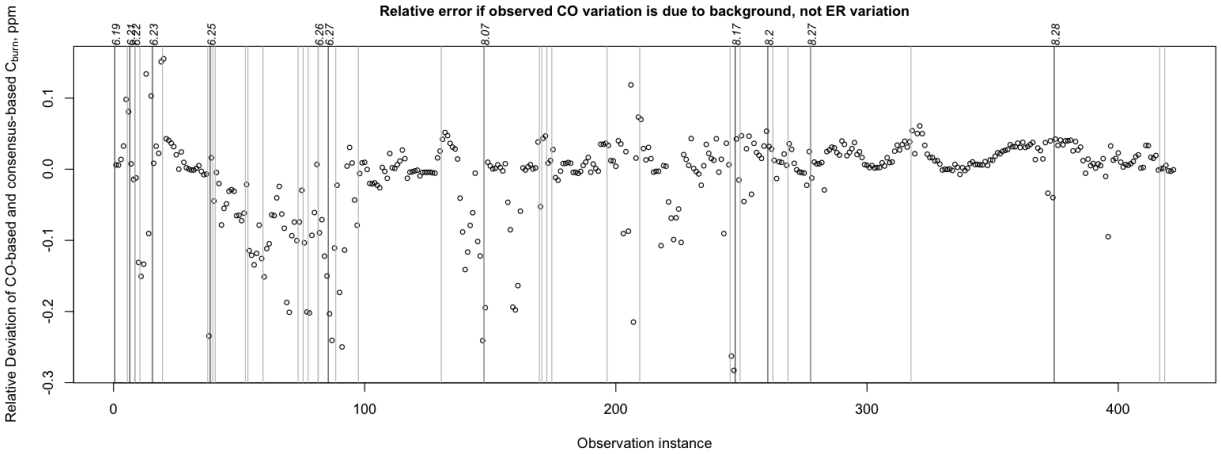

Figure S2 A heuristic measure of the stability of the situation.

The great variations in estimated $\hat{x}_i^0$ at a few points in Figure 9 can cause some concern (e.g. around sample numbered 8, 117, 130, 217m 231, 329, and 337) . Figure S2 suggests that sometimes these may be of concern, sometimes not. We constructed a measure of the temporal stability of the sampling situation by ratioing the changes of x0 to the amount of carbon burned, x-x0. The measure of change in ppm was

$$\text{Change Measure} = \left(\left|x_{i+1}^0 - x_i^0\right| + \left|x_i^0 - x_{i-1}^0\right|\right)/2$$

and to obtain a consistent measure of relative magnitude, an estimate of smoothed C_{burn} over the same span of i indices was also used,

$$\text{Magnitude Measure} = \left((x_{i-1} - x_{i-1}^0) + 2(x_i - x_i^0) + (x_{i+1} - x_{i+1}^0)\right)/4$$

This ratio of these gives our measure of the possible effect of relative change of actual C_{burn} during our the airborne measurements on the estimate of C_{burn} that the algorithm gives. Where the measurement crossed different plume boundaries (light gray lines in Figure 9), one-sided estimates consistent with these two values were calculated. We expect that use of absolute differences ratio may give a pessimistically high measure of potential influence; this was justified by a consideration of many different variations. The ratio Magnitude Measure / Change

Measure can reach high values, where changes in x_i^0 can be 0.2, 0.25, 0.33, and 0.5 the amount of C_{burn}, as the colors of the points in Figure 8 show. Recall, however, that the neighboring x_i^0 estimates and C_{burn} estimates are derived independently, so the ratio does not correspond to traditional measures of high-frequency noise, only the stability and relation to identifiable processes on the ground. Figure S2 suggests that for some periods of high C_{burn}, variations of x_i^0 should matter little in calculations of C_{burn} or of the ER ratios derived from C_{burn}. In other periods, when C_{burn} is low, there can be reason for concern, even when sample-to-sample variability of x_i^0 is not especially high.

Note on Examples of Enhancement Ratios (Section 8.1)

Methods used to prepare these graphs of EnRs for the two periods of observation, Figure S3 and Figure S4, are described in Sections.7 and 9.

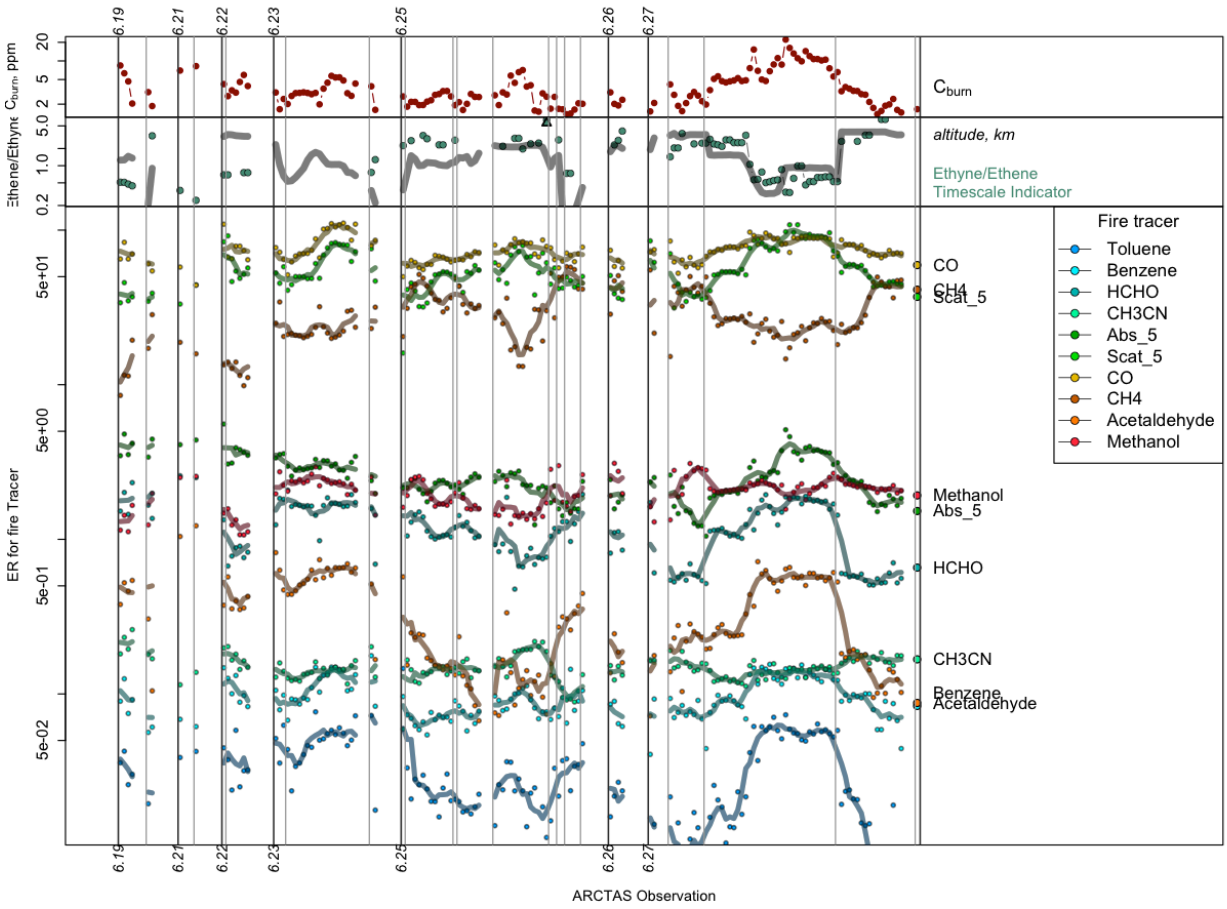

Figure S3. Estimates of C_{burn}, an ethyne/ethene photochemical transformation timescale, (Section 6.2), and enhancement ratios (EnRs) for each of the tracer compounds shown for all observations during the ARCTAS flights used in this analysis. Units for the EnRs are shown in Table 2. These diagrams were made using 10 tracers (including methane and methanol), not 8.

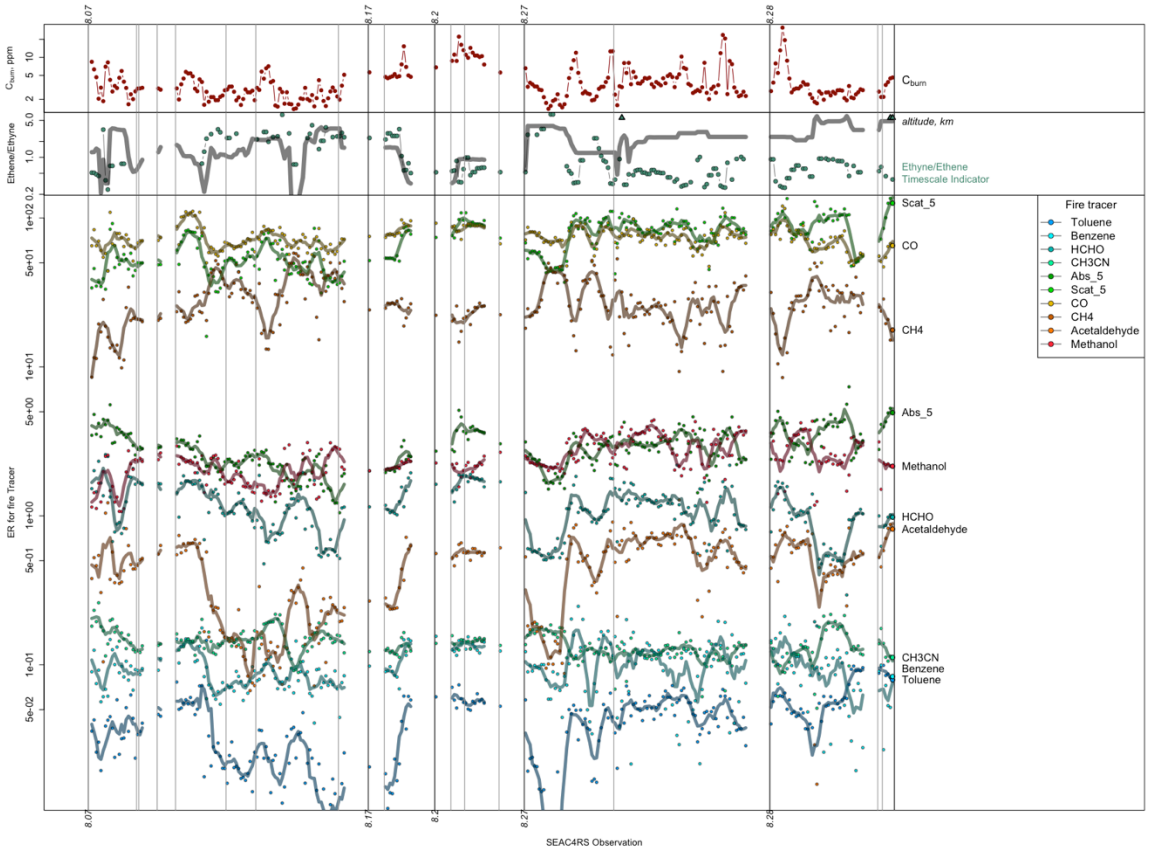

Figure S4. C_{bum} , an ethyne/ethene photochemical transformation timescale, (Section 6.2), and enhancement ratios (EnRs) for the SEAC4R observations. Units are given in Table 2.